

Neuron

Daily Oscillation of the Excitation-Inhibition Balance in Visual Cortical Circuits

Highlights

- The excitation/inhibition (E/I) ratio is dynamic across the 24-h day
- Fluctuations in the E/I ratio depend on sleep/wake history
- E/I ratio changes are circuit specific, not uniform across all synapses

Authors

Michelle C.D. Bridi, Fang-Jiao Zong, Xia Min, ..., Zheng-Jiang Zhu, Kai-Wen He, Alfredo Kirkwood

Correspondence

kwhe@sioc.ac.cn (K.-W.H.),
kirkwood@jhu.edu (A.K.)

In Brief

Bridi et al. investigate whether inhibition tracks known changes in excitation over the 24-h day to maintain a stable excitation/inhibition ratio. Surprisingly, the excitation/inhibition ratio is dynamic over the day in feedback, but not feedforward, visual cortical circuits.

Daily Oscillation of the Excitation-Inhibition Balance in Visual Cortical Circuits

Michelle C.D. Bridi,^{1,4} Fang-Jiao Zong,^{2,3,4} Xia Min,^{2,3} Nancy Luo,¹ Trinh Tran,¹ Jiaqian Qiu,^{2,3} Daniel Severin,¹ Xue-Ting Zhang,^{2,3} Guanglin Wang,² Zheng-Jiang Zhu,^{2,3} Kai-Wen He,^{2,3,*} and Alfredo Kirkwood^{1,5,*}

¹Mind/Brain Institute and Department of Neuroscience, Johns Hopkins University, Baltimore, MD 21218, USA

²Interdisciplinary Research Center on Biology and Chemistry, Shanghai Institute of Organic Chemistry, Chinese Academy of Sciences, Shanghai 200032, China

³University of Chinese Academy of Sciences, Beijing 100049, China

⁴These authors contributed equally

⁵Lead Contact

*Correspondence: kwhe@sioc.ac.cn (K.-W.H.), kirkwood@jhu.edu (A.K.)

<https://doi.org/10.1016/j.neuron.2019.11.011>

SUMMARY

A balance between synaptic excitation and inhibition (E/I balance) maintained within a narrow window is widely regarded to be crucial for cortical processing. In line with this idea, the E/I balance is reportedly comparable across neighboring neurons, behavioral states, and developmental stages and altered in many neurological disorders. Motivated by these ideas, we examined whether synaptic inhibition changes over the 24-h day to compensate for the well-documented sleep-dependent changes in synaptic excitation. We found that, in pyramidal cells of visual and prefrontal cortices and hippocampal CA1, synaptic inhibition also changes over the 24-h light/dark cycle but, surprisingly, in the opposite direction of synaptic excitation. Inhibition is upregulated in the visual cortex during the light phase in a sleep-dependent manner. In the visual cortex, these changes in the E/I balance occurred in feedback, but not feedforward, circuits. These observations open new and interesting questions on the function and regulation of the E/I balance.

INTRODUCTION

Cortical processing depends on the balanced interplay of glutamatergic excitatory synapses to propagate neural firing and GABAergic inhibitory synapses to limit propagation in time and space. The prevailing view is that the balance between synaptic excitation and inhibition (E/I balance) is maintained within a permissible window to ensure proper neural function (reviewed by Carandini and Heeger, 2011; Denève et al., 2017; Froemke, 2015; Isaacson and Scanziani, 2011; Keck et al., 2017; Rubin et al., 2017; Vogels et al., 2011). Therefore, a central question is how the E/I balance is regulated in neural circuits.

The importance of maintaining proper E/I balance in neural processing is underscored by studies showing that manipulating the E/I balance can disrupt social behavior and sensory perception (Ferguson and Gao, 2018; Shen et al., 2011; Yizhar et al., 2011). Moreover, numerous studies report E/I balance alterations in mouse models of neurological disorders, including autism and schizophrenia (Antoine et al., 2019; Gkogkas et al., 2013; Han et al., 2012, 2014; Tabuchi et al., 2007), Angelman and Rett syndromes (Calfa et al., 2015; Judson et al., 2016; Rotaru et al., 2018; Wallace et al., 2012), Alzheimer's disease (Busche and Konnerth, 2016; Busche et al., 2015), and tuberous sclerosis (Bateup et al., 2013). These changes in the E/I balance, largely due to changes in inhibition, are considered a primary contributing factor to the cognitive impairments associated with these pathologies (reviewed in Anticevic and Lisman, 2017; Nelson and Valakh, 2015; Rosenberg et al., 2015).

The notion that the E/I balance is maintained within an optimal range is supported by observations that the E/I ratio remains stable during neural development (Tao and Poo, 2005), between neighboring neurons (Xue et al., 2014), and transitioning within and between brain states (Zhou et al., 2014). In addition, synaptic homeostatic mechanisms are capable of maintaining the E/I balance within a target range, particularly during learning and cortical remodeling (D'amour and Froemke, 2015; Froemke, 2015; Nanou and Catterall, 2018).

These homeostatic mechanisms primarily affect the strength of inhibition in response to changes in excitation. In this context, it was of great interest that studies have shown marked sleep-dependent changes in cortical excitatory glutamatergic synapses at different times of the day (de Vivo et al., 2017; Diering et al., 2017; Gilestro et al., 2009; Liu et al., 2010; Maret et al., 2011; Vyazovskiy et al., 2008). We therefore asked whether changes in excitation over the day are compensated by complementary changes in inhibition to maintain the E/I balance. Surprisingly, we found that inhibition and excitation change in opposite directions over the 24-h day: when the frequency of excitatory synaptic events is high, the frequency of inhibitory events is low. These changes indicate a large oscillation of the E/I balance over the 24-h day, opening interesting questions as to how the E/I balance is regulated.

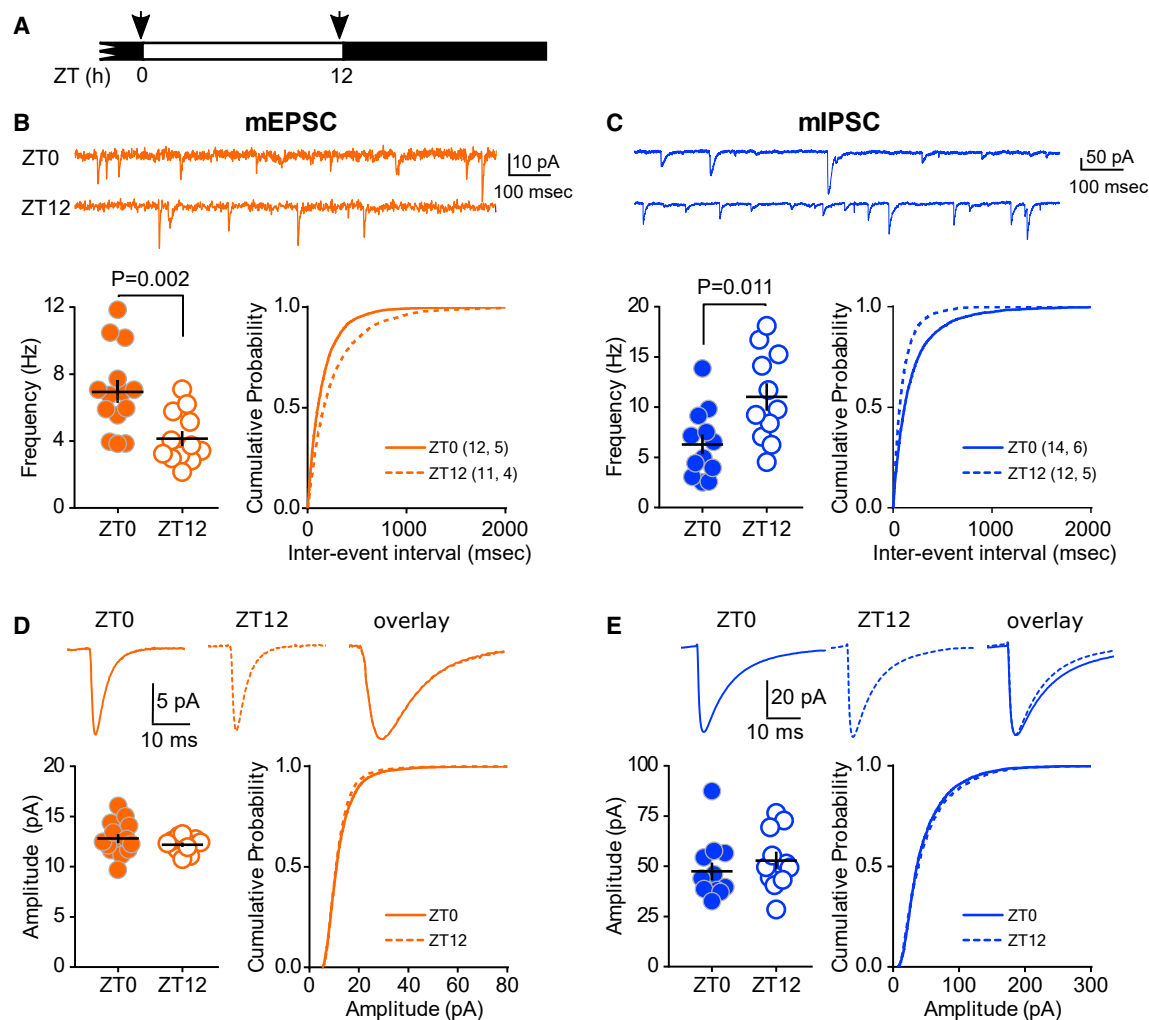


Figure 1. Opposite Changes in mEPSCs and mIPSCs over the Light/Dark Cycle in V1 L2/3 Pyramidal Cells

(A) Mice were entrained to a normal or reversed 12:12 L:D cycle for at least 2 weeks. Acute slices containing V1 were obtained at the end of the dark (ZT0) or light (ZT12) phase (arrowheads).

(B) mEPSC frequency was higher at ZT0 than ZT12. Top: example traces are shown. Bottom left: mEPSC frequency was higher at ZT0 than ZT12 (ZT0: 6.9 ± 0.7 Hz; ZT12: 4.2 ± 0.5 Hz; t test). Bottom right: there was a significant leftward shift in the cumulative probability histogram of the interevent intervals at ZT0 (Kolmogorov-Smirnov [KS]; $p < 0.0001$).

(C) mIPSC frequency was lower at ZT0 than ZT12. Top: example traces. Bottom: mIPSC frequency was significantly lower at ZT0 than ZT12 (left: ZT0: 6.3 ± 1.0 Hz; ZT12: 11.0 ± 1.4 Hz; t test), and the cumulative probability histogram showed a rightward shift (right: KS; $p < 0.0001$).

(D) mEPSC amplitude and kinetics did not differ between ZT0 and ZT12. Top: average traces of well-isolated events. Bottom: mEPSC amplitude was comparable (left: ZT0: 12.8 ± 0.4 pA; ZT12: 12.2 ± 0.2 pA; t test; $p = 0.8$). The distribution of individual event amplitudes was slightly but significantly different between groups (KS; $p = 0.009$).

(E) mIPSC amplitude and kinetics did not differ between ZT0 and ZT12. Top: average traces of well-isolated events. Bottom: mIPSC amplitude did not differ between groups (ZT0: 50.1 ± 5.0 pA; ZT12: 52.8 ± 4.4 pA; t test; $p = 0.7$). The cumulative distribution was slightly shifted leftward at ZT0 (KS; $p = 0.02$).

For all panels, mEPSC and mIPSC sample size is indicated as (cells, mice).

RESULTS

Modulation of Excitation and Inhibition in Opposite Directions across the 24-h Day

In the cortex, the number of spines and frequency of miniature excitatory synaptic events changes across the day in a sleep-dependent manner (Liu et al., 2010; Maret et al., 2011). These observations prompted us to examine whether compensatory

changes in synaptic inhibition maintain the E/I balance across the day. To that end, we recorded miniature excitatory postsynaptic currents (mEPSCs) and miniature inhibitory postsynaptic currents (mIPSCs) in layer 2/3 (L2/3) pyramidal cells of the primary visual cortex (V1) in slices harvested at the end of the dark (zeitgeber time [ZT] 0) and light (ZT12) phases (Figure 1A). Consistent with findings in the frontal cortex (Liu et al., 2010), in V1, the mEPSC frequency, but not amplitude (Figures 1B

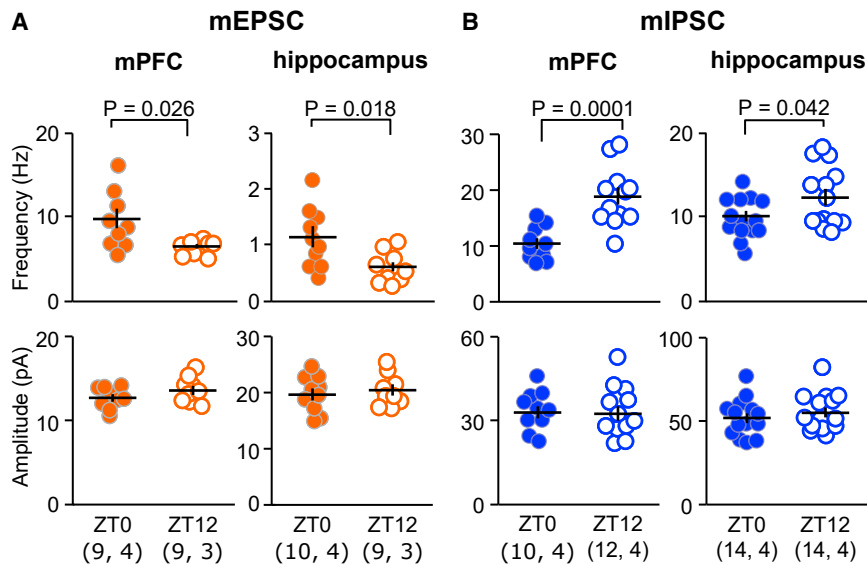


Figure 2. Pyramidal Cells in L2/3 Medial Prefrontal Cortex (mPFC) and Hippocampal CA1 Show the Same mEPSC and mIPSC Changes as V1

(A) mEPSC frequency, but not amplitude, was lower at ZT12 than ZT0. mPFC freq: ZT0 9.6 ± 1.2 Hz; ZT12 6.4 ± 0.3 Hz. CA1 freq: ZT0 1.1 ± 0.2 Hz; ZT12 0.6 ± 0.1 Hz. mPFC amp: ZT0 12.6 ± 0.4 pA; ZT12 13.6 ± 0.5 pA; $p = 0.15$. CA1 A: ZT0 19.6 ± 1.0 pA; ZT12 20.2 ± 1.0 pA; $p = 0.7$.

(B) mIPSC frequency, but not amplitude, was higher at ZT12 than ZT0 in mPFC and CA1. mPFC freq: ZT0 10.5 ± 1.0 Hz; ZT12 18.8 ± 1.5 Hz. CA1 freq: ZT0 9.9 ± 0.6 Hz; ZT12 12.3 ± 1.0 Hz. mPFC amp: ZT0 32.7 ± 2.3 pA; ZT12 32.3 ± 2.6 pA; $p = 0.9$. CA1 A: ZT0 55.2 ± 3.0 pA; ZT12 51.5 ± 3.0 pA; $p = 0.4$. Sample size indicated as (cells, mice).

and 1D), was higher in slices harvested at ZT0 than at ZT12. Inhibitory synaptic transmission also changed during the day but, surprisingly, in the opposite direction: mIPSC frequency was higher at ZT12 than at ZT0 (Figure 1C). As for mEPSCs, average mIPSC amplitude did not change (Figure 1E), although both cases showed a modest shift in the cumulative distributions of individual events at ZT12: leftward for mEPSCs and rightward for mIPSCs (Figures 1D and 1E). In addition to synaptic changes, alterations in neuronal excitability shape circuit function. We therefore measured maximal firing rate and action potential threshold in pyramidal cells and parvalbumin-positive (PV) interneurons. We detected no changes in either of these measures at different times of day (Figure S1).

These opposing changes in excitatory and inhibitory transmission were not restricted to V1. We observed similar changes in medial prefrontal cortex (mPFC) L2/3 and hippocampal CA1 (Figure 2), indicating that modulation of excitation and inhibition in opposite directions over the 24-h day may be a global phenomenon. Together, these results indicate that the ratio of mEPSC/mIPSC frequency, used as an indicator of the E/I balance (Han et al., 2012; Tabuchi et al., 2007), is not constant, as commonly assumed, but changes between ZT0 and ZT12.

Spontaneous sIPSCs Change across the Light/Dark Cycle in a Sleep- and Endocannabinoid-Signaling-Dependent Manner

We next quantified spontaneous IPSCs (sIPSCs) (in the absence of TTX and synaptic blockers) in V1, which better approximate natural conditions (Dani et al., 2005; Jurgensen and Castillo, 2015). We quantified inhibitory strength as the total charge (nC) in 1 s. To get a more detailed picture of how inhibitory synaptic transmission is modulated, we measured the inhibitory strength at six ZTs (Figure 3A). Consistent with mIPSCs, sIPSC charge at ZT12 was over twice that at ZT0. Notably, sIPSC charge was comparable across the light phase (ZT4, ZT8, and ZT12), suggesting a rapid upregulation of inhibition that stabilizes during

the light phase. Downregulation during the dark phase follows a similar temporal pattern. To investigate how rapidly upregulation occurs, we performed additional recordings at ZT1 (Figure S2A). At ZT1, sIPSC charge showed a nonsignificant increase compared to ZT0 and was significantly lower than at ZT4, suggesting that sIPSCs gradually increase between ZT0 and ZT4.

Sleep controls the daily changes in mEPSC frequency (Liu et al., 2010). Therefore, we asked whether this is also the case for inhibitory transmission. We tested whether sleep plays a role in the upregulation of the sIPSC charge between ZT0 and ZT4, when mice spend more time asleep. Mice were instrumented for polysomnography and divided into two groups. One group was sleep deprived (SD) by gentle handling for 4 h (ZT0–ZT4), and the other was allowed to sleep *ad libitum*; electroencephalogram (EEG) and electromyogram (EMG) recordings confirmed SD efficacy (Figure 3B). At ZT4, mice were sacrificed and sIPSCs were measured in V1 L2/3 pyramidal neurons. SD mice had significantly lower sIPSC charge compared to controls (Figure 3B). The magnitude of sIPSC charge in SD mice was comparable to ZT0 (Figure 3A), suggesting that sleep upregulates inhibition during the light phase.

Endocannabinoids (eCBs) suppress inhibitory transmission in the cortex (Fortin et al., 2004; Trettel and Levine, 2003; Trettel et al., 2004) and exhibit time-of-day variations in the rat brain (Murillo-Rodriguez et al., 2006; Valenti et al., 2004) and human plasma (Hanlon et al., 2016). Therefore, we tested whether signaling via cannabinoid receptors (CBRs) could be a mechanism to suppress sIPSCs during the dark phase. We collected slices at ZT0 or ZT12 and then pre-incubated and recorded slices in artificial cerebrospinal fluid (ACSF) containing either the CB1R antagonist SR 141716A (SR) or the CBR agonist WIN 55,212-2 (WIN). Inhibiting CB1R with SR at ZT0 increased inhibitory transmission to ZT12 levels, while SR had no effect at ZT12 (Figure 3C, left). The agonist WIN had the converse effect: WIN decreased inhibitory transmission at ZT12 but had

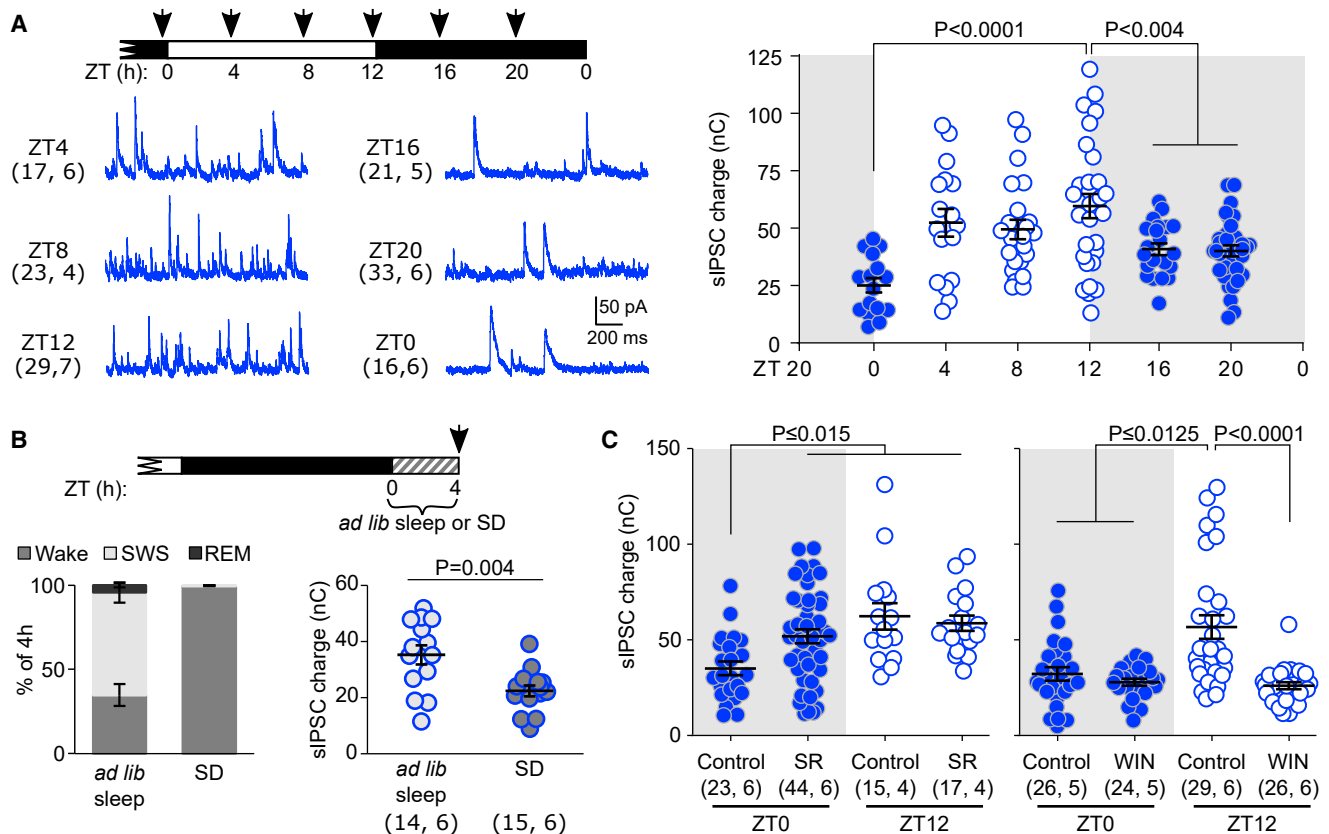


Figure 3. sIPSC Charge Oscillations across the Light/Dark Cycle Are Modulated by Sleep and CBR Signaling

(A) Left: acute brain slices were obtained at six different times of day (arrowheads). Representative traces show spontaneous IPSCs recorded at +10 mV with no drugs in the bath. Right: sIPSC charge was higher when the animal had been in the light phase prior to sacrifice. ZT0: 25.1 ± 3.2 nC; ZT4: 52.4 ± 6.0 nC; ZT8: 49.5 ± 4.2 nC; ZT12: 59.7 ± 5.3 nC; ZT16: 40.9 ± 2.5 nC; ZT20: 40.1 ± 2.4 nC. One-way ANOVA ($F(5, 133) = 7.6$; $p < 0.0001$); Holm-Sidak post hoc test.

(B) Mice underwent sleep deprivation (SD) or were allowed to sleep *ad libitum* for the first 4 h of the light cycle. Bottom left: EEG and EMG recordings confirmed the efficacy of the sleep deprivation. $n = 4$ mice/group. Bottom right: SD prevented the increase in sIPSCs that normally occurs between ZT0 and ZT4. Sleep: 35.2 ± 3.4 nC; SD: 22.4 ± 1.9 nC.

(C) Slices were obtained at ZT0 or ZT12 and pre-incubated with $10 \mu\text{M}$ SR or WIN in 0.1% DMSO for ≥ 1 h and then sIPSCs were recorded in the presence of drug. Slices from the same animals were used as controls (in 0.1% DMSO). SR increased sIPSC charge at ZT0, but not ZT12; conversely, WIN decreased sIPSCs at ZT12, but not ZT0. SR experiment: control ZT0: 35.2 ± 3.5 nC; SR ZT0: 51.9 ± 3.7 nC; control ZT12: 62.4 ± 7.0 nC; SR ZT12: 58.8 ± 4.0 nC; Kruskal-Wallis; $p = 0.0007$. WIN experiment: control ZT0: 32.3 ± 3.5 nC; WIN ZT0: 27.9 ± 1.8 nC; control ZT12: 56.7 ± 6.2 nC; WIN ZT12: 26.1 ± 1.8 nC; Kruskal-Wallis; $p < 0.0001$; Dunn's post hoc test.

For all panels, sample size is indicated as (cells, mice).

no effect at ZT0 (Figure 3C, right). Because CBR activation suppressed inhibitory transmission during the dark phase, we asked whether eCB levels are higher at this time of day. Mass spectrometry measurements of V1, hippocampus, and frontal cortex revealed higher levels of the most abundant eCB, 2-arachidonylglycerol (2-AG) (Hanlon et al., 2016), in the dark phase (Figure S2B). These results suggest that eCB signaling may be a mechanism to actively suppress inhibitory transmission during the dark phase.

Input-Specific Modulation of the E/I Ratio

Inhibitory interneurons in L2/3 participate in feedforward circuits driven by vertical ascending excitatory inputs, primarily from L4, and in feedback circuits driven by lateral inputs, primarily from L2/3. We therefore asked whether the E/I ratio changes be-

tween ZT0 and ZT12 in each of these pathways. Vertical inputs were stimulated optogenetically using a mouse expressing channelrhodopsin 2 (ChR2) specifically in L4; lateral stimulation was performed electrically (Figure 4A). We recorded evoked EPSCs and IPSCs in the same pyramidal cell by holding the membrane at the reversal potential for GABA and AMPA receptors, respectively (Figure S3). Because the E/I ratio varies with stimulation intensity (Morales et al., 2002), we stimulated each cell at a range of intensities to determine the range over which the E/I ratio is stable and used only values in this range for the analysis (Figure S3E).

With lateral stimulation, the E/I ratio was higher when the animal had been in the dark phase (ZT0 and ZT20) than when the animal had been in the light phase (ZT8 and ZT12; Figure 4B). This is consistent with the mEPSC, mIPSC, and sIPSC results

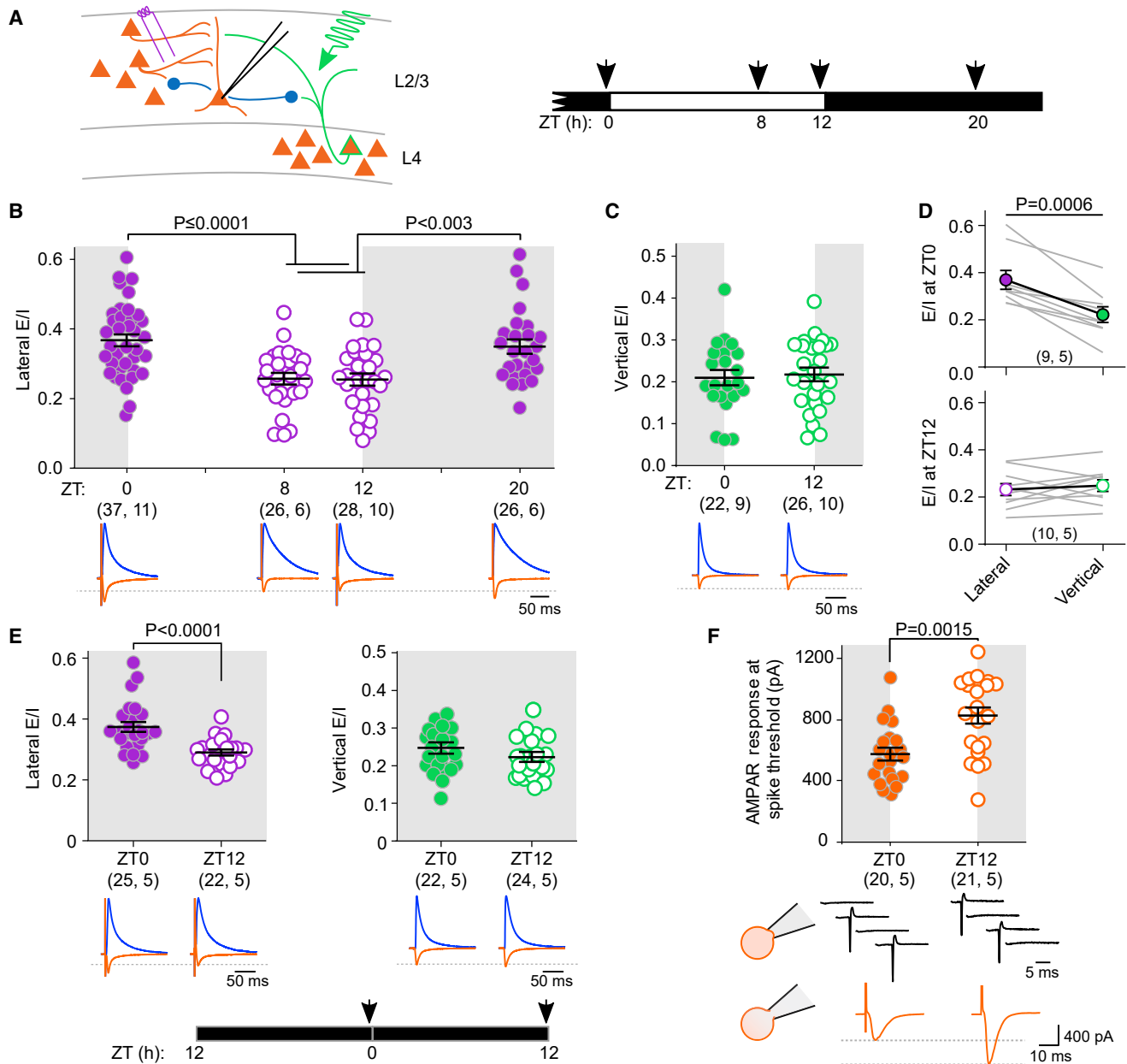


Figure 4. Circuit-Specific Modulation of the E/I Ratio

(A) Synaptic currents were evoked laterally by electrical stimulation in L2/3 or vertically by light-evoked release from ChR2-expressing L4 cells. L2/3 pyramidal cell responses were recorded in voltage clamp.

(B) The laterally evoked E/I ratio was higher when the animal had been in the dark phase prior to sacrifice (ZT0: 0.37 ± 0.02 ; ZT8: 0.26 ± 0.02 ; ZT12: 0.25 ± 0.02 ; ZT20: 0.35 ± 0.02 ; one-way ANOVA $F(3, 113) = 11.1$; $p < 0.0001$; post hoc Holm-Sidak test).

(C) The vertical E/I ratio did not change (ZT0: 0.20 ± 0.02 ; ZT12: 0.21 ± 0.02 ; t test $t(46) = 0.3$; $p = 0.75$).

(D) For a subset of cells in (B) and (C), we recorded responses to both vertical and lateral stimulation in the same cell. At ZT0, the lateral was higher than the vertical E/I ratio (paired t test $t(8) = 5.5$). At ZT12, the E/I ratio did not differ between pathways (paired t test $t(9) = 0.7393$; $p = 0.48$).

(E) Visual experience does not affect modulation of the E/I ratio. Mice were kept in complete darkness 24 h prior to experimentation. As in (B) and (C), the lateral E/I ratio was higher at ZT0 than at ZT12 (ZT0: 0.37 ± 0.02 ; ZT12: 0.29 ± 0.01 ; Mann-Whitney test $U(45) = 83$) and the vertical E/I ratio was unchanged (ZT0: 0.24 ± 0.01 ; ZT12: 0.22 ± 0.01 ; t test $t(44) = 1.3$; $p = 0.22$).

(F) Modulation of the lateral E/I ratio affects spike output. Cells were patched in cell-attached mode, and the lateral pathway was stimulated to identify spike threshold. The seal was then broken and the AMPA receptor response at spike threshold was recorded in whole-cell mode. At ZT12, more AMPA receptor current was required to reach threshold (ZT0: 570.1 ± 44.8 pA; ZT12: 817.3 ± 56.1 ; t test $t(39) = 3.4$).

In all panels, sample size is indicated as (cells, mice).

(Figures 1 and 3). We wished to confirm that these differences reflect the time of sacrifice, not changes in the E/I ratio in slices *ex vivo* over time. For each group, we examined the correlation between the time a cell was patched and the E/I ratio and found no correlation in any group (Figure S3H).

In contrast with lateral stimulation, the E/I ratio measured with vertical stimulation was not different between ZT0 and ZT12 (Figure 4C). This pathway-specific regulation of the E/I ratio was also observed when we examined a subset of experiments in which we measured both pathways in the same cell. At ZT0, the E/I ratio was larger with lateral than vertical stimulation. At ZT12, however, the E/I ratio was comparable in both pathways (Figure 4D).

Visual deprivation in the form of dark exposure specifically modulates lateral, but not vertical, inputs (Petrus et al., 2015), similar to the changes in the E/I ratio reported here (Figures 4B–4D). Therefore, we considered the possible role of visual experience over the light/dark cycle in the regulation of E/I balance. We exploited the fact that mice entrained to a 12:12 light:dark (L:D) cycle maintain their activity patterns for 5–7 days when placed in the dark (Faradji-Prevautelet et al., 1990). Therefore, 24 h prior to experimentation, we placed mice that had been on a 12:12 L:D cycle in constant and complete darkness to remove all visual experience. Similar to mice with normal experience, in visually deprived mice, the E/I ratio was larger at ZT0 than at ZT12 with lateral, but unchanged with vertical, stimulation (Figure 4E). Thus, the observed changes in E/I ratio across the light/dark cycle are not regulated by recent visual experience.

Finally, we explored whether the differences in lateral synaptic E/I ratio affect action potential firing, with the expectation that circuit excitability will be reduced when the E/I ratio is low. Therefore, we determined the amount of AMPA receptor current needed for each cell to reach spike threshold at ZT0 and ZT12. We held cells in cell-attached mode while stimulating the lateral pathway to identify the spike threshold (Figure 4F). Then, the seal was broken and the AMPA receptor current at spike threshold was recorded in whole-cell mode. More AMPA receptor current was required to reach spike threshold at ZT12, when the E/I ratio is low, than at ZT0 (Figure 4F). This is consistent with our finding that neurons do not compensate for changes in the synaptic E/I ratio with changes in excitability (Figure S1) and demonstrates that E/I fluctuations in the lateral circuit over the course of the day have a meaningful impact on spike output.

DISCUSSION

Maintaining the E/I balance within a permissive window is considered crucial to ensure proper neural processing. Here, we report that the E/I balance is not constant but changes markedly over the light/dark cycle. Over the course of the day, synaptic measures of excitation and inhibition change in opposite directions and in a sleep-dependent manner. Moreover, these changes are not uniform across cortical circuits. The E/I ratio of lateral inputs to L2/3 pyramidal cells changes, impacting neuronal spiking, but ascending inputs do not. These observa-

tions add complexity to our understanding of the E/I balance and pose intriguing questions.

The observation that the E/I ratio changes over the course of the day may seem to conflict with previous studies showing that, in cortical circuits, the E/I ratio remains constant across behavioral states (Tao and Poo, 2005; Xue et al., 2014; Zhou et al., 2014) and with the idea that experience-dependent cortical remodeling mechanisms return the E/I ratio to a target set point (Froemke, 2015). However, these ideas are not necessarily contradictory and can be reconciled if the set point for the E/I ratio slowly changes across the 24-h day. In this scenario, the E/I ratio within a short time window is dynamically maintained at the target set point by fast-acting correction mechanisms. Thus, at a particular time of day, the E/I value in a given circuit will be comparable across individuals and neural states. This explanation calls for plastic mechanisms operating at two distinct timescales: a fast (seconds to minutes) mechanism to correct deviations from the target set point and a slow (hours) one to modify the set point.

The mechanisms underlying the daily oscillation of the E/I balance remain to be fully understood and open questions on multiple levels. At the level of global arousal state, sleep promotes a decrease in excitation (de Vivo et al., 2017; Liu et al., 2010; Maret et al., 2011) and an increase in inhibition (Figure 3), but what drives the complementary process during the dark phase is less clear. At an elementary synaptic level, an intriguing aspect of the changes in E/I ratio is that they manifest in the frequency, not in amplitude, of mEPSCs and mIPSCs (Figures 1 and 2). This suggests a change in the number of synapses, not their potency, in agreement with sleep-dependent changes in the turnover of excitatory spines in cortex (Maret et al., 2011). This interpretation is also consistent with our findings that neither the paired-pulse ratio (a crude estimate of the release probability) nor the AMPA/NMDA ratio (a crude estimate of silent synapses) varies over the course of the day (Figure S3). Also consistent with this interpretation, molecular markers of GABAergic and glutamatergic synapses are higher during the light and dark phases, respectively, in the lateral hypothalamus and cerebellum (Cirelli et al., 2004; Laperchia et al., 2017; but see Del Cid-Pellitero et al., 2017). Besides structural changes, other mechanisms may also shape the E/I ratio. For example, neuromodulatory tone, which varies across arousal states, may control the spontaneous fusion of vesicles. Norepinephrine, which is high during waking, can directly increase the frequency of mEPSCs in the cortex (Choy et al., 2018), and mIPSC frequency can be affected by neuromodulation as well (Cilz and Lei, 2017; Gao et al., 2017; Madison and Nicoll, 1988). Here, we find that a potential contributing mechanism for suppression of inhibition in the dark phase is endocannabinoid signaling (Figure 3).

Intriguingly, changes in the E/I ratio occur specifically in the lateral, not feedforward, pathway (Figure 4). This agrees with our observations of spontaneous events, because the most abundant source of synaptic inputs to V1 L2/3 is lateral connections, not vertical inputs (Petrus et al., 2015). Interestingly, lateral, but not vertical, inputs are susceptible to long-term modification by prolonged altered sensory experience (Petrus

et al., 2015). Differences in E/I regulation between the two pathways may also reflect complex changes in the disynaptic circuitry, e.g., changes in excitatory inputs onto inhibitory interneurons, resulting in differential recruitment of inhibition. This scenario is in line with the observation that PV interneurons are differentially recruited across arousal states (Niethard et al., 2016).

Changes in excitation and inhibition over the 24-h day are a common feature across brain areas and have even been suggested in humans (Chellappa et al., 2016). Although the functional consequences of sleep-dependent increases in inhibitory synaptic transmission reported here remain to be determined, they dovetail with two major theories of sleep function. On one hand, enhanced inhibition may facilitate memory consolidation during sleep by improving spike timing precision. Precise timing of spikes in relation to hippocampal sharp-wave ripples is important for long-term potentiation during replay (Sadowski et al., 2016). On the other hand, increased inhibition promotes long-term depression (Steele and Mauk, 1999); hence, sleep may promote homeostatic weakening of excitatory synaptic transmission (Tononi and Cirelli, 2014). Finally, it is worth noting that alterations in the E/I ratio are thought to contribute to neural dysfunction. Notably, the difference in the E/I ratio between the dark and light phases reported here are comparable to the E/I alterations documented in models of autism (Antoine et al., 2019; Gkogkas et al., 2013; Han et al., 2012; Tabuchi et al., 2007). This opens the question of whether daily E/I cycling is dysregulated in these mouse models.

STAR★METHODS

Detailed methods are provided in the online version of this paper and include the following:

- [KEY RESOURCES TABLE](#)
- [LEAD CONTACT AND MATERIALS AVAILABILITY](#)
- [EXPERIMENTAL MODEL AND SUBJECT DETAILS](#)
 - Animals
- [METHOD DETAILS](#)
 - Slice Preparation
 - Whole-Cell Recording
 - Mass spectrometry analysis of 2-AG
 - Polysomnography recording
- [QUANTIFICATION AND STATISTICAL ANALYSIS](#)
 - Whole-cell recordings
 - Polysomnography
 - Statistics
- [DATA AND CODE AVAILABILITY](#)

SUPPLEMENTAL INFORMATION

Supplemental Information can be found online at <https://doi.org/10.1016/j.neuron.2019.11.011>.

ACKNOWLEDGMENTS

This work was supported by NIH grants R01EY012124 and R01EY025922 to A.K. and by NSFC grant 31700917 to K.-W.H. M.C.D.B. was supported by

NIH grant T32HL110952. K.-W.H. is supported by Thousand Youth Talents Program from Government of China.

AUTHOR CONTRIBUTIONS

Conceptualization and Writing, M.C.D.B., K.-W.H., and A.K.; Investigation, M.C.D.B., F.-J.Z., X.M., J.Q., X.-T.Z., G.W., K.-W.H., N.L., T.T., and D.S.; Funding Acquisition, A.K., Z.-J.Z., and K.-W.H.

DECLARATION OF INTERESTS

The authors declare no competing interests.

Received: February 14, 2019

Revised: September 16, 2019

Accepted: November 7, 2019

Published: December 9, 2019

REFERENCES

- Anticevic, A., and Lisman, J. (2017). How can global alteration of excitation/inhibition balance lead to the local dysfunctions that underlie schizophrenia? *Biol. Psychiatry* *81*, 818–820.
- Antoine, M.W., Langberg, T., Schnepel, P., and Feldman, D.E. (2019). Increased excitation-inhibition ratio stabilizes synapse and circuit excitability in four autism mouse models. *Neuron* *101*, 648–661.e4.
- Bateup, H.S., Johnson, C.A., Deneffrio, C.L., Saulnier, J.L., Kornacker, K., and Sabatini, B.L. (2013). Excitatory/inhibitory synaptic imbalance leads to hippocampal hyperexcitability in mouse models of tuberous sclerosis. *Neuron* *78*, 510–522.
- Busche, M.A., and Konnerth, A. (2016). Impairments of neural circuit function in Alzheimer's disease. *Philos. Trans. R. Soc. Lond. B Biol. Sci.* *371*, 20150429.
- Busche, M.A., Kekuš, M., Adelsberger, H., Noda, T., Förstl, H., Nelken, I., and Konnerth, A. (2015). Rescue of long-range circuit dysfunction in Alzheimer's disease models. *Nat. Neurosci.* *18*, 1623–1630.
- Calfa, G., Li, W., Rutherford, J.M., and Pozzo-Miller, L. (2015). Excitation/inhibition imbalance and impaired synaptic inhibition in hippocampal area CA3 of Mecp2 knockout mice. *Hippocampus* *25*, 159–168.
- Carandini, M., and Heeger, D.J. (2011). Normalization as a canonical neural computation. *Nat. Rev. Neurosci.* *13*, 51–62.
- Chellappa, S.L., Gaggioni, G., Ly, J.Q.M., Papachilleos, S., Borsu, C., Brzozowski, A., Rosanova, M., Sarasso, S., Luxen, A., Middleton, B., et al. (2016). Circadian dynamics in measures of cortical excitation and inhibition balance. *Sci. Rep.* *6*, 33661.
- Choy, J.M.C., Agahari, F.A., Li, L., and Stricker, C. (2018). Noradrenaline increases mEPSC frequency in pyramidal cells in layer II of rat barrel cortex via calcium release from presynaptic stores. *Front. Cell. Neurosci.* *12*, 213.
- Cilz, N.I., and Lei, S. (2017). Histamine facilitates GABAergic transmission in the rat entorhinal cortex: roles of H₁ and H₂ receptors, Na⁺-permeable cation channels, and inward rectifier K⁺ channels. *Hippocampus* *27*, 613–631.
- Cirelli, C., Gutierrez, C.M., and Tononi, G. (2004). Extensive and divergent effects of sleep and wakefulness on brain gene expression. *Neuron* *41*, 35–43.
- D'amour, J.A., and Froemke, R.C. (2015). Inhibitory and excitatory spike-timing-dependent plasticity in the auditory cortex. *Neuron* *86*, 514–528.
- Dani, V.S., Chang, Q., Maffei, A., Turrigiano, G.G., Jaenisch, R., and Nelson, S.B. (2005). Reduced cortical activity due to a shift in the balance between excitation and inhibition in a mouse model of Rett syndrome. *Proc. Natl. Acad. Sci. USA* *102*, 12560–12565.
- de Vivo, L., Bellesi, M., Marshall, W., Bushong, E.A., Ellisman, M.H., Tononi, G., and Cirelli, C. (2017). Ultrastructural evidence for synaptic scaling across the wake/sleep cycle. *Science* *355*, 507–510.

- Del Cid-Pellitero, E., Plavski, A., Mainville, L., and Jones, B.E. (2017). Homeostatic changes in GABA and glutamate receptors on excitatory cortical neurons during sleep deprivation and recovery. *Front. Syst. Neurosci.* *11*, 17.
- Denève, S., Alemi, A., and Bourdoukan, R. (2017). The brain as an efficient and robust adaptive learner. *Neuron* *94*, 969–977.
- Diering, G.H., Nirujogi, R.S., Roth, R.H., Worley, P.F., Pandey, A., and Huganir, R.L. (2017). Homer1a drives homeostatic scaling-down of excitatory synapses during sleep. *Science* *355*, 511–515.
- Faradji-Prevautel, H., Cespuglio, R., and Jouvet, M. (1990). Circadian rest-activity rhythms in the anophthalmic, monocular and binocular ZRDCT/An mice. Retinal and serotonergic (raphe) influences. *Brain Res.* *526*, 207–216.
- Ferguson, B.R., and Gao, W.-J. (2018). PV interneurons: critical regulators of E/I balance for prefrontal cortex-dependent behavior and psychiatric disorders. *Front. Neural Circuits* *12*, 37.
- Fortin, D.A., Trettel, J., and Levine, E.S. (2004). Brief trains of action potentials enhance pyramidal neuron excitability via endocannabinoid-mediated suppression of inhibition. *J. Neurophysiol.* *92*, 2105–2112.
- Froemke, R.C. (2015). Plasticity of cortical excitatory-inhibitory balance. *Annu. Rev. Neurosci.* *38*, 195–219.
- Gao, M., Whitt, J.L., Huang, S., Lee, A., Mihalas, S., Kirkwood, A., and Lee, H.K. (2017). Experience-dependent homeostasis of ‘noise’ at inhibitory synapses preserves information coding in adult visual cortex. *Philos. Trans. R. Soc. Lond. B Biol. Sci.* *372*, 20160156.
- Gilestro, G.F., Tsononi, G., and Cirelli, C. (2009). Widespread changes in synaptic markers as a function of sleep and wakefulness in *Drosophila*. *Science* *324*, 109–112.
- Gkogkas, C.G., Khoutorsky, A., Ran, I., Rampakakis, E., Nevarko, T., Weatherill, D.B., Vasuta, C., Yee, S., Truitt, M., Dallaire, P., et al. (2013). Autism-related deficits via dysregulated eIF4E-dependent translational control. *Nature* *493*, 371–377.
- Han, S., Tai, C., Westenbroek, R.E., Yu, F.H., Cheah, C.S., Potter, G.B., Rubenstein, J.L., Scheuer, T., de la Iglesia, H.O., and Catterall, W.A. (2012). Autistic behaviour in *Scn1a*^{+/-} mice and rescue by enhanced GABA-mediated neurotransmission. *Nature* *489*, 385–390.
- Han, S., Tai, C., Jones, C.J., Scheuer, T., and Catterall, W.A. (2014). Enhancement of inhibitory neurotransmission by GABAA receptors having $\alpha 2,3$ -subunits ameliorates behavioral deficits in a mouse model of autism. *Neuron* *81*, 1282–1289.
- Hanlon, E.C., Tasali, E., Leproult, R., Stuhr, K.L., Doncheck, E., de Wit, H., Hillard, C.J., and Van Cauter, E. (2016). Sleep restriction enhances the daily rhythm of circulating levels of endocannabinoid 2-arachidonoylglycerol. *Sleep (Basel)* *39*, 653–664.
- He, K., Huertas, M., Hong, S.Z., Tie, X., Hell, J.W., Shouval, H., and Kirkwood, A. (2015). Distinct Eligibility Traces for LTP and LTD in Cortical Synapses. *Neuron* *88*, 528–538.
- Isaacson, J.S., and Scanziani, M. (2011). How inhibition shapes cortical activity. *Neuron* *72*, 231–243.
- Judson, M.C.C., Wallace, M.L.L., Sidorov, M.S.S., Burette, A.C.C., Gu, B., van Woerden, G.M.M., King, I.F.F., Han, J.E.E., Zylka, M.J.J., Elgersma, Y., et al. (2016). GABAergic neuron-specific loss of *Ube3a* causes Angelman syndrome-like EEG abnormalities and enhances seizure susceptibility. *Neuron* *90*, 56–69.
- Jurgensen, S., and Castillo, P.E. (2015). Selective dysregulation of hippocampal inhibition in the mouse lacking autism candidate gene *CNTNAP2*. *J. Neurosci.* *35*, 14681–14687.
- Keck, T., Hübener, M., and Bonhoeffer, T. (2017). Interactions between synaptic homeostatic mechanisms: an attempt to reconcile BCM theory, synaptic scaling, and changing excitation/inhibition balance. *Curr. Opin. Neurobiol.* *43*, 87–93.
- Laperchia, C., Imperatore, R., Azeez, I.A., Del Gallo, F., Bertini, G., Grassi-Zucconi, G., Cristino, L., and Bentivoglio, M. (2017). The excitatory/inhibitory input to orexin/hypocretin neuron soma undergoes day/night reorganization. *Brain Struct. Funct.* *222*, 3847–3859.
- Liu, Z.-W., Faraguna, U., Cirelli, C., Tsononi, G., and Gao, X.-B. (2010). Direct evidence for wake-related increases and sleep-related decreases in synaptic strength in rodent cortex. *J. Neurosci.* *30*, 8671–8675.
- Madison, D.V., and Nicoll, R.A. (1988). Norepinephrine decreases synaptic inhibition in the rat hippocampus. *Brain Res.* *442*, 131–138.
- Maret, S., Faraguna, U., Nelson, A.B., Cirelli, C., and Tsononi, G. (2011). Sleep and waking modulate spine turnover in the adolescent mouse cortex. *Nat. Neurosci.* *14*, 1418–1420.
- Morales, B., Choi, S.-Y., and Kirkwood, A. (2002). Dark rearing alters the development of GABAergic transmission in visual cortex. *J. Neurosci.* *22*, 8084–8090.
- Murillo-Rodríguez, E., Désarnaud, F., and Prospéro-García, O. (2006). Diurnal variation of arachidonylethanolamine, palmitoylethanolamide and oleoylethanolamide in the brain of the rat. *Life Sci.* *79*, 30–37.
- Nanou, E., and Catterall, W.A. (2018). Calcium channels, synaptic plasticity, and neuropsychiatric disease. *Neuron* *98*, 466–481.
- Nelson, S.B., and Valakh, V. (2015). Excitatory/inhibitory balance and circuit homeostasis in autism spectrum disorders. *Neuron* *87*, 684–698.
- Niethard, N., Hasegawa, M., Itokazu, T., Oyanedel, C.N., Born, J., and Sato, T.R. (2016). Sleep-stage-specific regulation of cortical excitation and inhibition. *Curr. Biol.* *26*, 2739–2749.
- Petrus, E., Rodriguez, G., Patterson, R., Connor, B., Kanold, P.O., and Lee, H.-K. (2015). Vision loss shifts the balance of feedforward and intracortical circuits in opposite directions in mouse primary auditory and visual cortices. *J. Neurosci.* *35*, 8790–8801.
- Rosenberg, A., Patterson, J.S., and Angelaki, D.E. (2015). A computational perspective on autism. *Proc. Natl. Acad. Sci. USA* *112*, 9158–9165.
- Rotaru, D.C., van Woerden, G.M., Wallaard, I., and Elgersma, Y. (2018). Adult *Ube3a* gene reinstatement restores the electrophysiological deficits of prefrontal cortex layer 5 neurons in a mouse model of Angelman syndrome. *J. Neurosci.* *38*, 8011–8030.
- Rubin, R., Abbott, L.F., and Sompolinsky, H. (2017). Balanced excitation and inhibition are required for high-capacity, noise-robust neuronal selectivity. *Proc. Natl. Acad. Sci. USA* *114*, E9366–E9375.
- Sadowski, J.H.L.P., Jones, M.W., and Mellor, J.R. (2016). Sharp-wave ripples orchestrate the induction of synaptic plasticity during reactivation of place cell firing patterns in the hippocampus. *Cell Rep.* *14*, 1916–1929.
- Shen, W., McKeown, C.R., Demas, J.A., and Cline, H.T. (2011). Inhibition to excitation ratio regulates visual system responses and behavior in vivo. *J. Neurophysiol.* *106*, 2285–2302.
- Steele, P.M., and Mauk, M.D. (1999). Inhibitory control of LTP and LTD: stability of synapse strength. *J. Neurophysiol.* *81*, 1559–1566.
- Tabuchi, K., Blundell, J., Etherton, M.R., Hammer, R.E., Liu, X., Powell, C.M., and Südhof, T.C. (2007). A neuroligin-3 mutation implicated in autism increases inhibitory synaptic transmission in mice. *Science* *318*, 71–76.
- Tao, H.W., and Poo, M.M. (2005). Activity-dependent matching of excitatory and inhibitory inputs during refinement of visual receptive fields. *Neuron* *45*, 829–836.
- Tsononi, G., and Cirelli, C. (2014). Sleep and the price of plasticity: from synaptic and cellular homeostasis to memory consolidation and integration. *Neuron* *81*, 12–34.
- Trettel, J., and Levine, E.S. (2003). Endocannabinoids mediate rapid retrograde signaling at interneuron right-arrow pyramidal neuron synapses of the neocortex. *J. Neurophysiol.* *89*, 2334–2338.
- Trettel, J., Fortin, D.A., and Levine, E.S. (2004). Endocannabinoid signalling selectively targets perisomatic inhibitory inputs to pyramidal neurones in juvenile mouse neocortex. *J. Physiol.* *556*, 95–107.
- Tu, J., Yin, Y., Xu, M., Wang, R., and Zhu, Z.J. (2017). Absolute quantitative lipidomics reveals lipidome-wide alterations in aging brain. *Metabolomics* *14*, 5.
- Valenti, M., Viganò, D., Casico, M.G., Rubino, T., Steardo, L., Parolaro, D., and Di Marzo, V. (2004). Differential diurnal variations of anandamide and 2-arachidonoyl-glycerol levels in rat brain. *Cell. Mol. Life Sci.* *61*, 945–950.

Vogels, T.P., Sprekeler, H., Zenke, F., Clopath, C., and Gerstner, W. (2011). Inhibitory plasticity balances excitation and inhibition in sensory pathways and memory networks. *Science* 334, 1569–1573.

Vyazovskiy, V.V., Cirelli, C., Pfister-Genskow, M., Faraguna, U., and Tononi, G. (2008). Molecular and electrophysiological evidence for net synaptic potentiation in wake and depression in sleep. *Nat. Neurosci.* 11, 200–208.

Wallace, M.L., Burette, A.C., Weinberg, R.J., and Philpot, B.D. (2012). Maternal loss of *Ube3a* produces an excitatory/inhibitory imbalance through neuron type-specific synaptic defects. *Neuron* 74, 793–800.

Xue, M., Atallah, B.V., and Scanziani, M. (2014). Equalizing excitation-inhibition ratios across visual cortical neurons. *Nature* 511, 596–600.

Yizhar, O., Fenno, L.E., Prigge, M., Schneider, F., Davidson, T.J., O’Shea, D.J., Sohal, V.S., Goshen, I., Finkelstein, J., Paz, J.T., et al. (2011). Neocortical excitation/inhibition balance in information processing and social dysfunction. *Nature* 477, 171–178.

Zhou, M., Liang, F., Xiong, X.R., Li, L., Li, H., Xiao, Z., Tao, H.W., and Zhang, L.I. (2014). Scaling down of balanced excitation and inhibition by active behavioral states in auditory cortex. *Nat. Neurosci.* 17, 841–850.

STAR★METHODS

KEY RESOURCES TABLE

REAGENT or RESOURCE	SOURCE	IDENTIFIER
Chemicals, Peptides, and Recombinant Proteins		
tetrodotoxin citrate	Abcam	Cat # AB120055
DL-AP5	Tocris	Cat # 0105
Bicuculline methiodide	Enzo	Cat # BML-EA149-0050
SR-95531 (gabazine)	Sigma-Aldrich	Cat # S106
WIN 55,212-2 mesylate	Cayman Chemical	Cat # 10009023
Rimonabant Hydrochloride (SR 141716A)	Abmole	Cat # M7325
CNQX disodium salt hydrate	Sigma Aldrich	Cat # C239
NBQX disodium salt hydrate	Sigma Aldrich	Cat # N183
Adenosine 5'-triphosphate magnesium salt	Sigma Aldrich	Cat # A9187
Guanosine 5' Triphosphate Sodium Salt Hydrate	Sigma Aldrich	Cat # G8877
Lidocaine N-ethyl Bromide (QX-314)	Sigma Aldrich	Cat # L5783
Phosphocreatine disodium salt hydrate	Sigma Aldrich	Cat # P7936
2-arachidonoyl glycerol (2-AG)	Cayman Chemical	Cat # 62160
MTBE (LC grade)	MilliporeSigma	Cat # 101845
Critical Commercial Assays		
Pierce BCA protein assay kit	ThermoFisher	Cat # 23225
Experimental Models: Organisms/Strains		
B6 mouse: C57BL/6J	The Jackson Laboratory	RRID:IMSR_JAX:000664
L4-cre mouse: B6;C3- Tg(Scnn1a-cre)3Aibs/J	The Jackson Laboratory	RRID:IMSR_JAX:009613
Ai32 mouse: B6;129S- <i>Gt(ROSA)26Sor^{tm32(CAG-COP4*H134R/EYFP)Hze}/J</i>	The Jackson Laboratory	RRID:IMSR_JAX:012569
Software and Algorithms		
Prism	GraphPad	RRID:SCR_002798
IgorPro	Wavemetrics	RRID:SCR_000325
Mini Analysis	Synaptosoft	RRID:SCR_002184
MATLAB R2016a	MathWorks	RRID:SCR_001622
Ponemah/Neuroscore	DSI	RRID:SCR_017107
MATLAB code for sIPSC analysis	this paper	https://github.com/michellebridi/sIPSC
MassHunter Quantitative Analysis	Agilent Technologies	RRID:SCR_015040

LEAD CONTACT AND MATERIALS AVAILABILITY

Further information and requests for resources and reagents should be directed to and will be fulfilled by the lead contact, Alfredo Kirkwood (kirkwood@jhu.edu). This study did not generate new unique reagents.

EXPERIMENTAL MODEL AND SUBJECT DETAILS

Animals

All procedures were approved by the Institutional Animal Care and Use Committees at Johns Hopkins University and/or the Interdisciplinary Research Center on Biology and Chemistry, Chinese Academy of Science.

Mice were group housed in standard cages on a 12h:12 h light/dark cycle. Naive 5-10 week old mice of either sex were used. C57BL/6J mice were bred in-house and used for all experiments, except for experiments in which L4 was optogenetically stimulated, in which case mice specifically expressing Chr2 in L4 were generated by crossing B6;C3- Tg(Scnn1a-cre)3Aibs/J and B6;129S-*Gt(ROSA)26Sor^{tm32(CAG-COP4*H134R/EYFP)Hze}/J* mice (The Jackson Laboratory, Bar Harbor, ME). The time the lights were turned on (ZT0) was adjusted according to the experiment. Mice with shifted light/dark cycles were entrained in a customized entraining

chamber for at least 2 weeks before experiments. Whenever possible, within a given experiment, littermates were distributed across experimental groups.

METHOD DETAILS

Slice Preparation

300 μm thick coronal brain slices containing either V1, mPFC, or transverse sections of hippocampus were prepared as described previously (He et al., 2015). Briefly, slices were cut in ice-cold dissection buffer containing 212.7 mM sucrose, 5 mM KCl, 1.25 mM NaH_2PO_4 , 10 mM MgCl_2 , 0.5 mM CaCl_2 , 26 mM NaHCO_3 , and 10 mM dextrose, bubbled with 95% O_2 /5% CO_2 (pH 7.4). Slices were transferred to normal artificial cerebrospinal fluid (similar to the dissection buffer except that sucrose was replaced by 119 mM NaCl, MgCl_2 was lowered to 1 mM, and CaCl_2 was raised to 2 mM) and incubated at 30 °C for 30 min and then at room temperature for at least 30 min before recording.

Whole-Cell Recording

Visualized whole-cell recordings were made from pyramidal neurons in L2/3 (35% depth from the pia) of V1 and mPFC, and CA1. Glass pipette recording electrodes (3–5 $\text{M}\Omega$) were filled with different internal solutions according to each experiment, all of which were adjusted to pH 7.2–7.3, 280–295 mOsm. Cells with an input resistance $\geq 100 \text{ M}\Omega$ and access resistance $\leq 25 \text{ M}\Omega$ were recorded. For all whole cell recordings, cells were discarded if these values changed more than 25% during the experiment. Data were filtered at 2 kHz for voltage clamp and 10 kHz for current clamp and digitized at 10 kHz using either Igor Pro (WaveMetrics) or Clampex (Axon).

Miniature and spontaneous postsynaptic current recordings

For mEPSC recordings, 1 μM TTX, 100 μM DL-APV and 10 μM bicuculline or 10 μM gabazine were added to the perfusion buffer to isolate AMPAR-mediated mEPSCs. An internal pipette solution containing the following ingredients was used: 8 mM KCl, 125 mM cesium gluconate, 10 mM HEPES, 1 mM EGTA, 4 mM MgATP, 0.5 mM NaGTP, and 5 mM QX-314. V_m was held at -70 mV .

To record spontaneous IPSCs, the internal solution was similar except no QX-314 was added, no drugs were included in the bath, and V_m was held at $+10 \text{ mV}$. To test the effects of endocannabinoid signaling on sIPSCs, slices were pre-incubated for at least 1 h in either 10 μM (+)-WIN55,212-2 (Cayman Chemical, Ann Arbor, MI) or SR 141716A (Abmole, Pudong New Area, Shanghai, China) in 0.1% DMSO. These drugs were also present in the bath during sIPSC recording. Control slices were obtained from the same animal and control ACSF contained 0.1% DMSO. In a subset of SR sIPSC recordings, DMSO was excluded from the control bath and DL-APV was included, but this did not affect sIPSC charge (t test $p > 0.50$) so the data were pooled.

To record mIPSCs, 1 μM TTX, 100 μM DL-APV and 20 μM CNQX or NBQX were included in the bath. The internal pipette solution contained: 8 mM NaCl, 120 mM cesium chloride, 10 mM HEPES, 2 mM EGTA, 4 mM MgATP, 0.5 mM NaGTP, and 10 mM QX-314. V_m was held at -70 mV .

Evoked E/I

The internal solution for recording evoked EPSCs and IPSCs was identical to that used for mEPSCs and responses were recorded in the presence of 100 μM APV. The reversal potential for excitatory and inhibitory currents were measured to be $+10 \text{ mV}$ and -55 mV without compensating for the junction potential (Figure S3). To evoke synaptic response from lateral synapses, a double-barrel glass stimulating pipette filled with regular ACSF was placed about 100 μm lateral to the recording electrode. Vertical inputs from L4 were stimulated optogenetically by activating Chr2 with blue light. For both stimulation methods, a series of stimulations over a range of intensities was delivered to generate an input-output curve for both EPSCs and IPSCs. Only the responses within the linear range of both I-O curves (stable E/I ratio) were used to calculate the evoked E/I ratio.

AMPA/NMDA ratio

L2/3 pyramidal neurons were voltage-clamped in whole-cell configuration. Recordings were made in standard ACSF containing gabazine (2.5 μM) and glycine (1 μM); to decrease polysynaptic activity, Ca^{2+} and Mg^{2+} concentrations were increased to 4 mM and adenosine (10 μM) was added to the bath. The internal pipette solution contained (in mM): 102 cesium gluconate, 5 TEA-chloride, 3.7 NaCl, 20 HEPES, 0.2 EGTA, 10 BAPTA, 0.3 Na-guanosine triphosphate, 4 Mg-adenosine triphosphate, and 5 QX-314 bromide. Synaptic responses were evoked with a stimulating electrode placed laterally to the recording pipette within L2/3. Evoked synaptic responses were recorded at -80 mV and $+40 \text{ mV}$ holding potentials. The stimulus intensity was set as 2x the threshold to evoke a response at -80 mV , and cells with polysynaptic responses were excluded.

Intrinsic excitability

L2/3 pyramidal neurons were current-clamped at -70 mV with K^+ -based internal solution containing (in mM): 130 (K) gluconate, 10 KCl, 0.2 EGTA, 10 HEPES, 4 (Mg) ATP, 0.5 (Na) guanosine triphosphate, and 10 (Na) phosphocreatine. The perfusion buffer contained 100 μM DL-APV, 20 μM CNQX or NBQX, and 10 μM bicuculline. A 1 s ramp test with injected current from 20–1000 pA was used to estimate the spiking threshold membrane potential and minimal current. Injection of 1 s current steps (50, 100, 150, 200, 400, 600, 800, 1000, 1200, 1400 pA), cycled 2–3 times was used to find the maximal firing rate. Only cells with resting membrane potentials $\leq -65 \text{ mV}$, access resistance $\leq 25 \text{ M}\Omega$, and input resistance $> 85 \text{ M}\Omega$ were used.

Mass spectrometry analysis of 2-AG

Brain tissue sample preparation

6 week old C57BL/6J mice were anesthetized and sacrificed between either ZT 9-11 (Light) or ZT 21-23 (Dark). Frontal cortex, hippocampus, and visual cortex were quickly dissected out and frozen immediately in liquid N₂. Tissue was kept at –80°C until the day of sample preparation. Lipids from brain tissue were extracted using a modified MTBE (MilliporeSigma, Burlington, MA) extraction method as described before (Tu et al., 2017). Briefly, frozen brain tissue was weighed and homogenized with ddH₂O (~200 μl H₂O for ~20 mg tissue) using the Precellys 24 homogenizer (5500 rpm, 3x20 s, repeat 3 times, Bertin Technologies, France). Protein concentration was then measured with Pierce BCA Protein Assay Kit (Thermo Fisher) and samples from the same brain region were normalized with ddH₂O to the same concentration. 100 μl of homogenized solution was mixed with 300 μl ddH₂O and 960 μl extraction solvent (MTBE:MeOH = 5:1, v/v), and then vortexed for 60 s followed by 10 min of sonication. Then the mixture was centrifuged at 13000 rpm for 15 min. After collection the upper organic layer, 500 μl MTBE was added to the bottom layer for re-extraction. The re-extraction was repeated twice. The pooled organic layer was evaporated using a vacuum concentrator. The dry extract was reconstituted using 100 μl of DCM:MeOH (1:1, v/v) prior to LC-MS/MS analysis.

LC-MS/MS analysis

The LC-MS analysis was performed using an HPLC system (1260 series, Agilent Technologies, Santa Clara, CA) coupled to a triple quadrupole mass spectrometer (Agilent QqQ 6495, Agilent Technologies). A Phenomenex Kinetex C8 column (50 × 2.1 mm; particle size, 2.6 μm; 100Å) was used for separation. The mobile phase A and mobile phase B were 100% H₂O with 0.1% formic acid and 100% ACN with 0.1% formic acid, respectively. The linear gradient was kept at 1% B for the first min, and eluted from 1% to 99% B (1-8 min), stayed at 99% B for one min (8-9 min), then eluted from 99% to 1% B (10.0-10.1 min), and finally kept at 1% B for 1.9 min (10.1-12.0 min). The flow rate was 0.5 mL/min and the sample injection volume was 2 μL. The measurement was performed in positive mode. ESI source parameters were set as followings: sheath gas temperature, 350°C; dry gas temperature, 250°C; sheath gas flow, 12 L/min; dry gas flow, 12 L/min; capillary voltage, 3500V in positive mode; nozzle voltage, 1500 V in positive mode; and nebulizer pressure, 20 psi. For the analyses of 2-AG, three MRM transitions were simultaneously monitored, including 379.3/287.2 for quantification, 379.3/91.0 for qualification, 379.3/79.0 qualification. The dwell time for each MRM transition is 150 ms. The MRM transitions were obtained using purchased chemical standard of 2-AG (Cayman Chemical) (100 μg/mL), and optimized using the MassHunter Optimizer software (Agilent Technologies). The external calibration curve was also measured for the quantification of 2-AG ranging from 1, 5, 25, 100, 500, 1000, 2000, to 5000 ng/ml. The external calibration curve was run twice at the beginning and the end of the acquisition batch. The peak areas of quantification transition (i.e., 379.3/287.2) were plotted using a linear least square regression with a weight of 1/x using the MassHunter Quantitative Analysis software (Agilent Technologies). The 2-AG amounts in biological samples were quantified using the measured peak areas through the interpolation from the calibration curve.

Polysomnography recording

Surgery

8-9 week old C57BL/6J mice were anesthetized by isoflurane (1%–2%) and head-fixed. The skull was exposed for implanting two epidural screw EEG electrodes over the visual cortex (B: –3–4mm, L: 2-3 mm). Two resin-insulated stainless steel wires bared at the tip region were implanted into the dorsal neck muscles and sutured in place to record the electromyogram (EMG). All electrodes were connected to a 4-pin socket connector that was glued to the skull by dental cement. After surgery, the wound was treated with triple antibiotic ointment and the mice were allowed to recover in their home cage for at least 7 days before the experiment. Mice were transferred to the customized chamber 1 day before the recording for habituation.

During recording, all signals were amplified (Differential AC amplifier, model 1700, A-M systems) and digitized at 500 Hz by Spike Hound. EEG and EMG signals were bandpass filtered (1-500 Hz and 1-1000 Hz, respectively).

Sleep deprivation

Mice implanted for polysomnography were individually housed on a 12h/12h light/dark cycle (lights on at 8 am). On the day of experiment, the arousal states of 1 control (Sleep *ad lib*) and 1 sleep-deprived (SD) mouse were monitored side-by-side from 8 am to 12 pm. The control mouse was allowed to sleep *ad libitum*, while the SD mouse was enforced to stay awake by gentle handling.

QUANTIFICATION AND STATISTICAL ANALYSIS

Whole-cell recordings

Spontaneous events

mEPSCs and mIPSCs were analyzed using the MiniAnalysis program (Synaptosoft, Decatur, GA). Only cells with root mean square (RMS) noise < 2 (mEPSCs) or < 4 (mIPSCs) were included in the analysis and event detection threshold was set at 3 times the RMS noise. 300 events with rise time < 3 msec (mEPSCs) or < 5 msec (mIPSCs) were selected for each cell to calculate frequency and amplitude. Non-overlapping events were used to construct the averaged traces.

Spontaneous IPSCs were analyzed by calculating the unit charge (nC/s) with custom code (MATLAB, MathWorks, Inc, Natick, MA). The baseline was calculated and subtracted for each 500 msec of recording. Charge was calculated as the integral of the baseline-subtracted signal. 3-4 min of recording were quantified for each cell.

Evoked responses

For E/I ratio measurements, peak response amplitude at each holding potential was measured for each stimulus intensity and the ratio between the excitatory and inhibitory peak was calculated (Igor Pro, Wavemetrics). If multiple peaks were observed in the post-synaptic response, we used the magnitude of the first peak in order to limit the analysis to monosynaptic responses. If the first peak could not be clearly resolved, the cell was discarded from the analysis. For AMPA/NMDA measurements, the AMPA receptor-mediated response was measured as the peak magnitude at -80 mV and the NMDA component of the response at $+40$ mV was measured 70 msec after stimulation. If the response had multiple peaks the cell was excluded from the analysis.

Polysomnography

Arousal stages were scored offline manually by visual inspection of 10 s epochs (Neuroscore, DSI). Amount of time spent in each of three arousal states (SWS, REM, and wake) was quantified and compared between the sleep and SD groups.

Statistics

All data were analyzed with 2-tailed t tests, Wilcoxon rank-sum tests, ANOVAs with Holm-Sidak posthoc analysis, or Kruskal-Wallis with Dunn's posthoc analysis, as indicated in the figure legends (GraphPad Prism, San Diego, CA). Cumulative distributions were compared with the Kolmogorov-Smirnov (KS) test. $p < 0.05$ was considered significant. The D'Agostino-Pearson test was used to assess normality; in cases where data were not normally distributed, nonparametric tests were used. Sample size is displayed in the figures as (number of cells, number of animals). Lines and error bars in all figure dot plots indicate mean and SEM.

DATA AND CODE AVAILABILITY

The MATLAB code used to analyze the sIPSC data generated during this study is available on Github [<https://github.com/michellebridi/sIPSC>].